Pramana – J. Phys. (2021) 95:108
https://doi.org/10.1007/s12043-021-02144-7

Properties of pure neutron matter at low and high densities

KH GAD[1,2]

[1]Physics Department, Faculty of Science, Islamic University of Madinah, Madinah, Kingdom of Saudi Arabia
[2]Physics Department, Faculty of Science, Sohag University, Sohâg 82524, Egypt
E-mail: khalafgad@yahoo.com

MS received 2 March 2020; revised 12 September 2020; accepted 12 March 2021

Abstract. We report a new microscopic equation of state (EoS) of pure neutron matter (PNM) at zero temperature using the recent realistic two-body interaction derived in the framework of chiral perturbation theory (ChPT). The EoS is derived using the Brueckner–Bethe–Goldstone quantum many-body theory in the Brueckner–Hartree–Fock approach. We have calculated the EoS of PNM at low and high densities using LO, NLO, N^{2}LO, N^{3}LO, N^{4}LO potentials at three different values of the momentum-space cut-off Λ = 450, 500 and 550 MeV. It is found that the EoS is not much affected by the cut-off variations at low densities. Also the binding energy of PNM has been computed within the framework of the Brueckner–Hartree–Fock (BHF) approach plus two-body density-dependent Skyrme potential which is equivalent to three-body forces. The effect of the two-body density-dependent Skyrme potential is to produce a stiffer EoS. This is actually needed to improve the saturation point of symmetric nuclear matter obtained using the two-body NN interaction. The results of several microscopic approaches are compared. It is found that the EoS is sensitive to the momentum-space cut-off Λ. Also the partial wave contributions to potential energy at the empirical saturation density $\rho = 0.16$ fm^{-3} for different potentials are listed from $^1S_0$ to $^3F_3$ states. It is found that all contributions are nearly cut-off independent except the ones from $^3P_1$, $^3P_2$, $^3H_4$ and $^3F_4$ states, which are increasing with the cut-off Λ. Actually, the size of these contributions is strongly dependent on the central and tensor components in the NN potential. The larger cut-off Λ corresponds to harder interactions and gives more repulsive contribution to the NN potential at short distance. It leads to smaller binding energy.

Keywords. Neutron matter; Skyrme force; Brueckner–Hartree–Fock approach; continuous choice.

PACS Nos **26.60.+c; 24.10.Cn; 13.75.Cs**

1. Introduction

The properties of pure neutron matter (PNM) are important for addressing a number of open questions in nuclear physics, astrophysics and the structure of neutron stars [1–12]. The structure of neutron stars is strongly sensitive to the equation of state (EoS) [13–15]. Also the study of EoS of PNM [16–21] has attracted a lot of attention because it is a crucial input for modelling neutron stars and supernovae [1,14]. In the inner core of the neutron stars, the baryon number density may reach 5–10 times the nuclear saturation density ρ_0, where the deconfinement hadron–quark phase transition may occur [22,23]. Also the mass of a neutron star depends mainly on the EoS of the neutron matter.

It is well accepted that modern nucleon–nucleon interactions cannot describe the binding energies of nuclei with $A \leq 3$. This drawback is usually overcome by including three-body forces (TBF) or by a correction term equivalent to TBF. The TBF plays a very important role in nuclear physics, because it is essential to reproduce the empirical saturation point of symmetric nuclear matter (SNM) ($\rho_0 = 0.16 \pm 0.01$ fm^{-3}, $\frac{E}{A}|_{\rho_0} = -16.0 \pm 1$ MeV) and to give an adequately stiff EoS which is consistent with the present measured neutron star masses and in particular with the mass $M = 2.01 \pm 0.04 M_\odot$ [2] of the neutron star in PSR J0348 + 0432. The TBF is not very important at very small densities, but at high densities it is very important.

The inclusion of TBF was considered by many researchers. In ref. [24], the BHF results for both neutron and symmetric nuclear matter were implemented by the inclusion of the Urbana TBF [25,26]. The addition of a correction term (CT) can provide sufficient repulsion which is consistent with all the constraints.

The NN potentials employed in this work span five orders in the chiral effective field theory (EFT) expansion [27–31], from leading order (LO) to fifth order (N^4LO) and different values of the momentum-space cut-off Λ where we shall take $\Lambda = 450$, 500 and 550 MeV. The same power counting scheme and regularisation procedures are applied through all orders, making this set of interactions more consistent than the previous ones. Another novel and important aspect in the construction of these new potentials is the fact that the long-range part of the interaction is fixed by the πN low-energy constants (LECs) as determined in the recent and very accurate analysis of Hoferichter *et al* [32]. In fact, for all practical purposes, errors in the πN LECs are no longer an issue with regard to uncertainty quantification.

In the present study, in order to establish the importance of the two-body density-dependent Skyrme potential which is equivalent to three-body forces (TBF) in the calculation of EoS for PNM our aim is to extend the Brueckner–Hartree–Fock (BHF) approach which ignores the TBF to BHF+CT approach, which includes the two-body density-dependent Skyrme potential. The results are compared with various many-body approaches. The plan of this article is as follows: After the introductory remarks, we briefly review the theoretical background in §2. The results and discussions are presented in §3, while conclusions are given in §4.

2. The theoretical model

2.1 *BHF approach for PNM*

In this subsection we briefly illustrate how to evaluate, in the BHF approximation [33–43], the energy per neutron of a system of pure neutrons. The basic ingredient is the Brueckner G-matrix, which is the solution of the Bethe–Goldstone equation

$$G(\rho,\omega) = v + v\sum_{k_1k_2}\frac{|k_1k_2\rangle\, Q_{k_1,k_2}\langle k_1k_2|}{\omega-\varepsilon_{k_1}-\varepsilon_{k_2}}\; G(\rho,\omega), \quad (1)$$

where v is the free neutron–neutron interaction, ω is the starting energy of the interacting neutron and Q is the Pauli operator which prevents scattering into occupied states. The single-particle energy ε_k (assuming $\hbar = 1$) is given as

$$\varepsilon_k = \frac{k^2}{2m_n} + U(k,\rho), \quad (2)$$

where the single-particle potential $U(k)$ using the continuous choice prescription is

$$U(k,\rho) = \mathrm{Re}\sum_{k'\le k_F}\langle kk'|G(\rho,\omega{=}\varepsilon_k{+}\varepsilon_{k'})|kk'\rangle_a, \quad (3)$$

where the subscript a indicates antisymmetrisation of the matrix element. In this scheme, the only input quantity we need is the bare NN interaction, v, in the Bethe–Goldstone equation (1). In this work, we adopt the new LO, NLO, N^2LO, N^3LO and N^4LO potentials [27–31] as a model for the free two-neutron interaction.

In order to obtain such a self-consistent solution of the BHF equations, one often assumes a quadratic dependence of the single-particle energy on the momentum of the neutron in the form

$$\varepsilon_k \approx \frac{k^2}{2m_n^*} + C, \quad (4)$$

where m_n^* is the effective mass of the neutron matter and C is a constant.

In PNM, only partial waves with a pair of interacting nucleons coupled to isospin $T = 1$ contribute to the calculation of G-matrix. Due to the antisymmetry of the matrix elements, only partial waves with even values for the sum $L + S$, like $^1S_0$, $^3P_0$, etc. are considered [22]. In the case of symmetric nuclear matter (SNM), the other partial waves, like $^3S_1 - {}^3D_1$ and $^1P_1$ contribute.

Once a self-consistent solution of eqs (1) and (3) is obtained for different densities, the energy per neutron can be easily calculated as

$$\frac{E}{A} = \frac{3}{5}\frac{k_F^2}{2m_n} + \frac{1}{2\rho}\mathrm{Re}\sum_{k,k'\le k_F}\langle kk'|G(\rho,\omega = \varepsilon_k + \varepsilon_{k'})|kk'\rangle_a. \quad (5)$$

Also the pressure is defined in term of the energy per nucleon as

$$P(\rho,\alpha) = \rho^2\frac{\partial(E/A)}{\partial\rho}. \quad (6)$$

Also the energy of the non-interacting Fermi gas is given as

$$\frac{E_{FG}}{N} = \frac{3}{5}\frac{k_F^2}{2m}. \quad (7)$$

2.2 *The Skyrme model*

It is well known that the two-body forces (2BF) cannot explain some nuclear properties. For example, the BHF calculations, based on 2BF, fail to reproduce the correct saturation point for symmetric nuclear matter [44]. They either predict too small binding energy at the empirical value for the density, or about the correct energy at a density, which is too large by a factor of two, or results in between ('Coester band' [44]). Also for finite nuclei,

Table 1. Parameters t_0, t_3 and x_3 defining the contact interaction of eq. (11) as obtained for the fit to the saturation point $\rho = 0.16\ \text{fm}^{-3}$ and $E/A = -16$ MeV at $\alpha = 0.5$ for BHF approach.

	t_0 (MeV fm^3)	t_3 (MeV fm$^{3+3\alpha}$)	x_3
At $\Lambda = 450$ MeV			
LO	−24.3	16.9	19.56
NLO	−264.58	4343.75	−0.17266105
N^{2}LO	−243.75	4281.25	−0.19214465
N^{3}LO	−233.75	4306.25	−0.24963653
N^{4}LO	−250.0	4500.0	−0.229166
At $\Lambda = 500$ MeV			
LO	302.08	−4406.25	−0.15177224
NLO	−262.58	4073.75	−0.1159917
N^{2}LO	−222.83	3832.5	−0.2625565
N^{3}LO	−215.83	3762.5	−0.202325
N^{4}LO	−218.0	3742.5	−0.15531
At $\Lambda = 550$ MeV			
LO	1860.0	−26725.0	−0.05547129
NLO	−256.67	3775.0	−0.33774857
N^{2}LO	−227.917	3768.75	−0.2971803
N^{3}LO	−231.67	3900.0	−0.2564097
N^{4}LO	−241.4583	4021.875	−0.2657648

it is well accepted that modern nucleon–nucleon interactions cannot describe the binding energies of nuclei with mass number $A \geq 3$, and they have to be combined with three-body forces (TBF) [45]. TBF terms or density-dependent two-nucleon interactions are needed to achieve saturation in symmetric nuclear matter. Also, different ways have been developed to obtain expectations for the properties of nuclear systems under exotic conditions. One way is to start from phenomenological models which successfully describe the properties of stable nuclei. A very popular approach along this line is the use of an effective density-dependent Skyrme-type interaction which has frequently been described in refs [46–49]. The total energy of a nucleus can be expressed as the integral of the energy density functional $\mathcal{H}$ [50]

$$E = \int \mathcal{H}(r)\,\mathrm{d}r, \tag{8}$$

where $\mathcal{H}$ is the Hamiltonian density in the Hartree–Fock approximation. Energy density functional $\mathcal{H}(r)$ for Skyrme interaction can be split into various contributions [51]

$$\mathcal{H} = \mathcal{K} + \mathcal{H}_{\text{eff}} + \mathcal{H}_0 + \mathcal{H}_3, \tag{9}$$

where $\mathcal{K}$ is the kinetic energy term, $\mathcal{H}_{\text{eff}}$ is an effective mass-dependent term, $\mathcal{H}_0$ is a zero range term and $\mathcal{H}_3$ is a density-dependent term, which are pertinent for calculating the properties of nuclear matter. These terms are given by

$$\begin{aligned}
\mathcal{K} &= \frac{\hbar^2}{2m}\tau,\\
\mathcal{H}_{\text{eff}} &= \frac{1}{8}\big[t_1(2+x_1) + t_2(2+x_2)\big]\tau\rho\\
&\quad + \frac{1}{8}\big[t_2(2x_2+1) - t_1(2x_1+1)\big]\big[\tau_p\rho_p + \tau_n\rho_n\big],\\
\mathcal{H}_0 &= \frac{1}{4}t_0\big[(2+x_0)\rho^2 - (2x_0+1)(\rho_p^2+\rho_n^2)\big],\\
\mathcal{H}_3 &= \frac{1}{24}t_3\rho^\alpha\big[(2+x_3)\rho^2 - (2x_3+1)(\rho_p^2+\rho_n^2)\big],
\end{aligned} \tag{10}$$

where ρ_n and ρ_p are the neutron and proton densities respectively and the total density $\rho = \rho_n + \rho_p$ (in the case of PNM, $\rho_p = 0$ so $\rho = \rho_n$). Also the coefficients t_i, x_i, W_0 and α are parameters of a generalised Skyrme force.

The extension of the BHF approach to include correction term can be found in refs [52–54]. Therefore, it is quite natural to supplement the self-energy of BHF calculations by a simple contact interaction (CT), which we have chosen following the notation of the Skyrme interaction to be the form,

$$\Delta\mathcal{H} = \text{CT} = (\mathcal{H}_0 + \mathcal{H}_3)/\rho. \tag{11}$$

The parameters of the contact interaction are t_0, x_0, t_3, x_3 and α. As described below we have chosen a fixed value of $x_0 = 0.0$ and $\alpha = 0.5$, and fitted t_0, t_3 and x_3 in such a way that BHF calculations plus the contact interaction term (CT) of eq. (11) yield both the empirical saturation point of the SNM (at $\rho = 0.16\,\text{fm}^{-3}$, $E/A = -16.0$ MeV, $P = 0.0$) and reproduce the symmetry energy at saturation density (at $\rho = 0.16\,\text{fm}^{-3}$, $E_{\text{sym}} = 32.0$

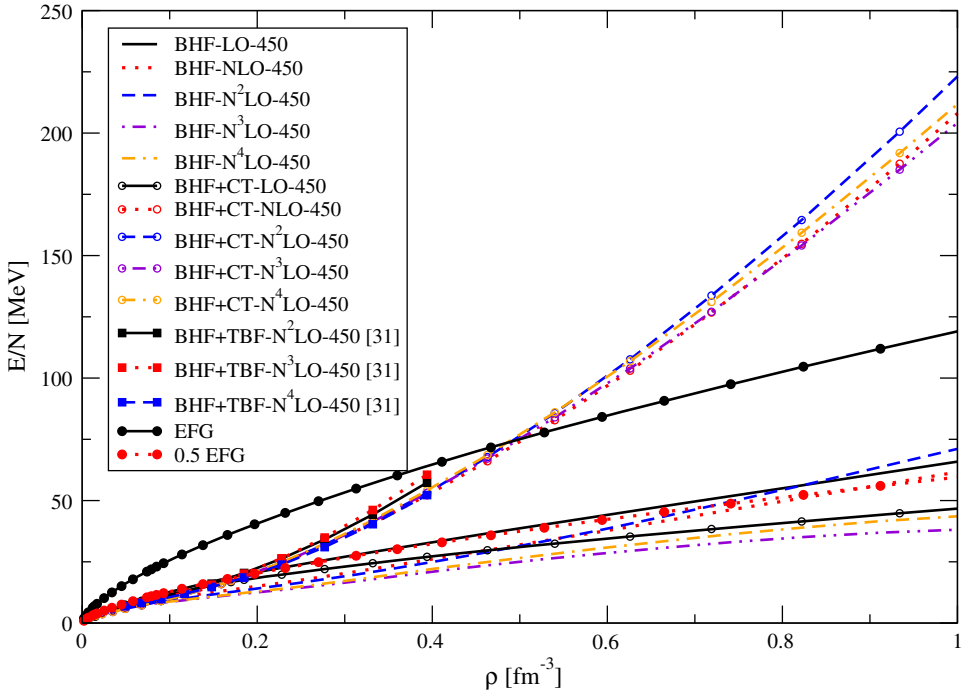

Figure 1. The EoS of PNM as a function of density using various potentials. The predictions are obtained from BHF and BHF+CT calculations. The cut-off Λ is fixed at 450 MeV. The results are compared with the EoS obtained with the BHF+TBF [31] and compared with Fermi gas and half Fermi gas.

MeV) in table 1 for LO, NLO, N^2LO, N^3LO and N^4LO potentials. Note that this CT is isoscalar and does not affect the effective masses.

3. Results and discussions

We have made the usual angular average on the Pauli operator as well as on the energy denominator in the propagator [55], in order to perform a partial wave expansion of the Bethe–Goldstone equation (1). For each calculation, we have included all partial wave contributions up to a total two-body angular momentum $J_{\max} = 8$. Actually, the contributions coming from higher partial waves are completely negligible.

In figures 1–3 the density behaviour of the energy per neutron of PNM is calculated in the BHF and BHF+CT approximations using LO, NLO, N^2LO, N^3LO and N^4LO potentials at the momentum-space cut-off $\Lambda =$ 450, 500, 550 MeV respectively.

The differences between various energies are smaller in PNM, especially at low and medium densities. This is mainly due to the absence of the ${}^3S_1 - {}^3D_1$ contribution. In PNM, the strong nuclear tensor force contribution from the $T = 0$ channel is absent. The important ${}^3S_1 - {}^3D_1$ channel does not contribute to the energy per neutron. Therefore, the difference between various potentials is expected to be small, especially at low and medium densities. This is very similar to the case reported by Li *et al* [56] in a neutron matter calculation.

At lower densities, the five potentials produce very close binding energies per neutron, which proves that all potentials yield the same on-shell T-matrix. At higher densities, the quenching mechanisms due to the Pauli operator and the energy denominator (second term in Bethe–Goldstone equation (1)) account for the differences in binding exhibited by the five potentials. The potential N^3LO producing the weakest tensor force is the most attractive. The binding energy of the N^3LO potential is the smallest of the five potentials. As can be concluded from figure 1, the predictions from the N^4LO calculation are close to the half Fermi gas energy at least up to saturation densities.

One can see that the binding energies are highly sensitive to the choice of nuclear force and often turn out to be too large. This has recently been observed by Sammarruca *et al* [31] and Binder *et al* [60]. The TBF is soft and on its own would lead to substantial overbinding in nuclear matter, but the addition of a repulsive CT contribution leads to a much better description of the nuclear matter saturation point. The inclusion of CT or TBF is necessary beyond about half nuclear matter saturation density.

In figure 1, we compare our results with the results obtained with the BHF+TBF [31]. The repulsion given by the addition of TBF is evident, which becomes

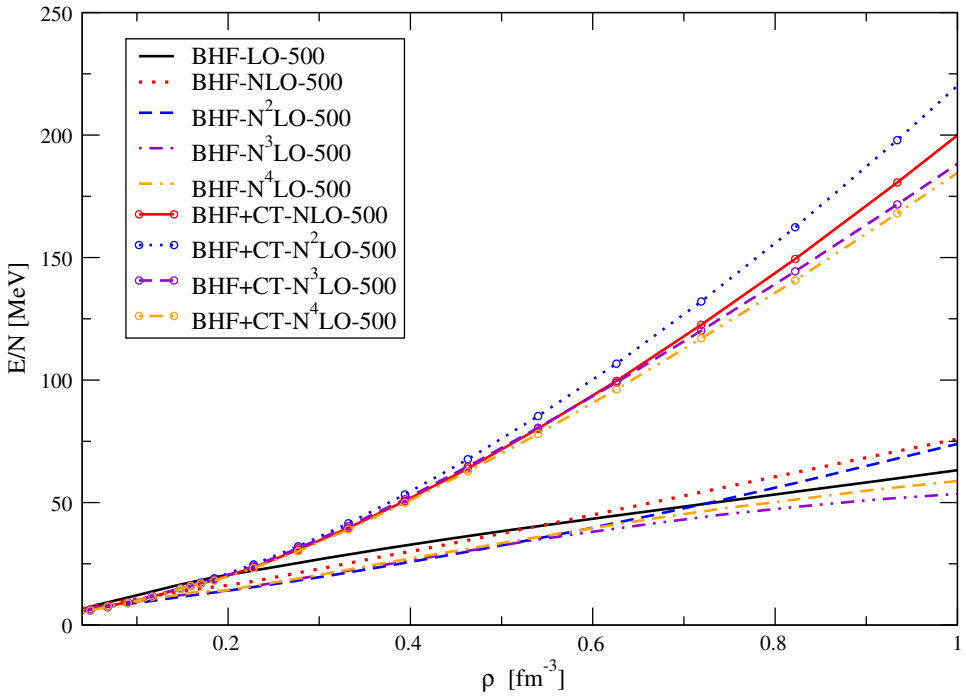

Figure 2. The EoS of PNM as a function of density using various potentials. The predictions are obtained from BHF and BHF+CT calculations. The cut-off Λ is fixed at 500 MeV.

negligible at low densities. As the density increases, the repulsive contribution of the TBF increases rapidly. This is very similar to those obtained by Akmal *et al* using the AV18 potential [58]. There is a very good agreement between our results using BHF+CT and those calculated in the BHF+TBF approach [31] over large density ranges.

We also compare our results with Fermi gas and half Fermi gas. In the low density region, the Fermi gas was larger than the BHF+CT, whereas it is the opposite at high densities. Half Fermi gas is in agreement with BHF calculation.

In figure 4 we show the binding energy per neutron as a function of density for LO, NLO, N^2LO, N^3LO and N^4LO potentials at the momentum-space cut-off $\Lambda = 450, 500, 550$ MeV. The final potential appears more repulsive at high density for the N^2LO than for the N^3LO potential. Generally, our results for PNM show an increasing attraction in the NN force when going from LO to N^2LO that can probably be traced back to the two-pion exchange potential (TPEP), which has a very strong attractive central isoscalar piece. At N^3LO, the chiral TPEP receives further attractive contributions and also develops a repulsive short-range core. The additional repulsion at N^4LO comes from the contributions to the TPEP at this order. These results indicate that the differences in the prediction of the EoS at high densities are not only due to the many-body method used, but also due to the various models used for the NN interaction. The effect of the momentum-space cut-off is evident at high densities, and becomes negligible at low densities.

At very low densities, the EoS of PNM is determined by the s-wave (spin = 0 and isospin = 1) [61] neutron–neutron interaction. Also, at very low densities, neutron matter is very similar to cold Fermi atoms near unitarity (infinite scattering length), because two free neutrons are very nearly bound [45].

In tables 2 and 3, we compare the contributions from various partial wave channels to the potential energy of PNM. We show the momentum space cut-off Λ dependence for three selected aspects that are of great interest at $\rho = 0.16$ fm^{-3} for chiral NLO, N^2LO, N^3LO and N^4LO potentials. The partial wave channels are listed from $^1S_0$ to $^3F_4$ states. It is found that except the ones from $^3P_1$ and $^1D_2$ which are decreasing with increasing the cut-off Λ. The larger cut-off Λ corresponds to harder interactions and gives more repulsive contribution to the NN potential at short distance. It leads to smaller binding energy. We can make the interesting observation that the reproduction of NN observables is not much affected by the cut-off variations.

By comparing the results using the three different cut-off values Λ, one may notice that the discrepancy between the total binding energies calculated mainly comes from the P, H and F channels. In the case of symmetric nuclear matter, the discrepancy between the

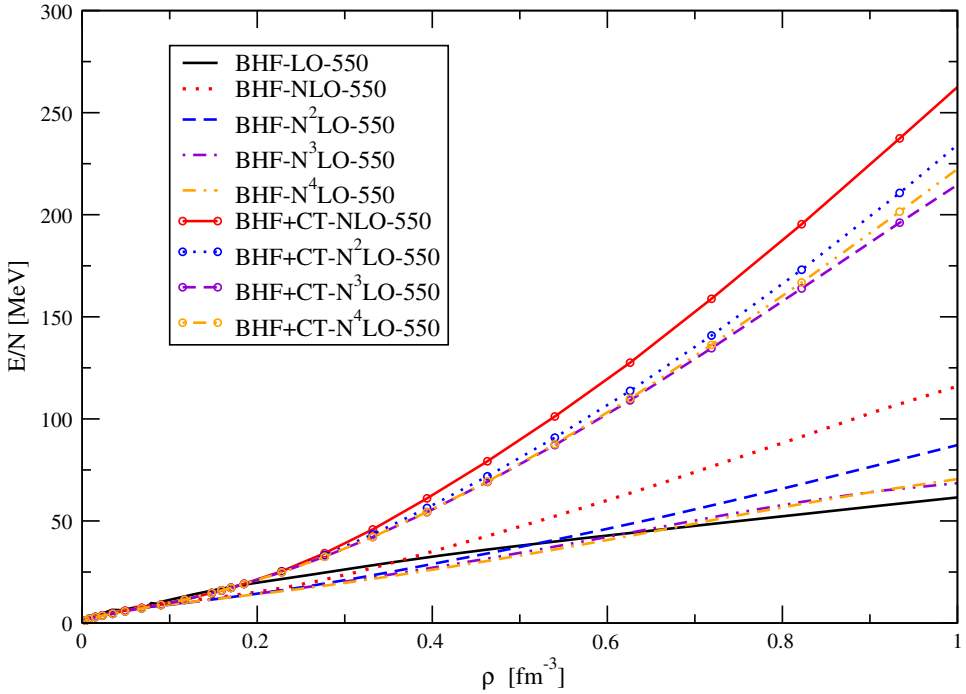

Figure 3. Same as figure 2 but using momentum-space cut-off $\Lambda = 550$ MeV.

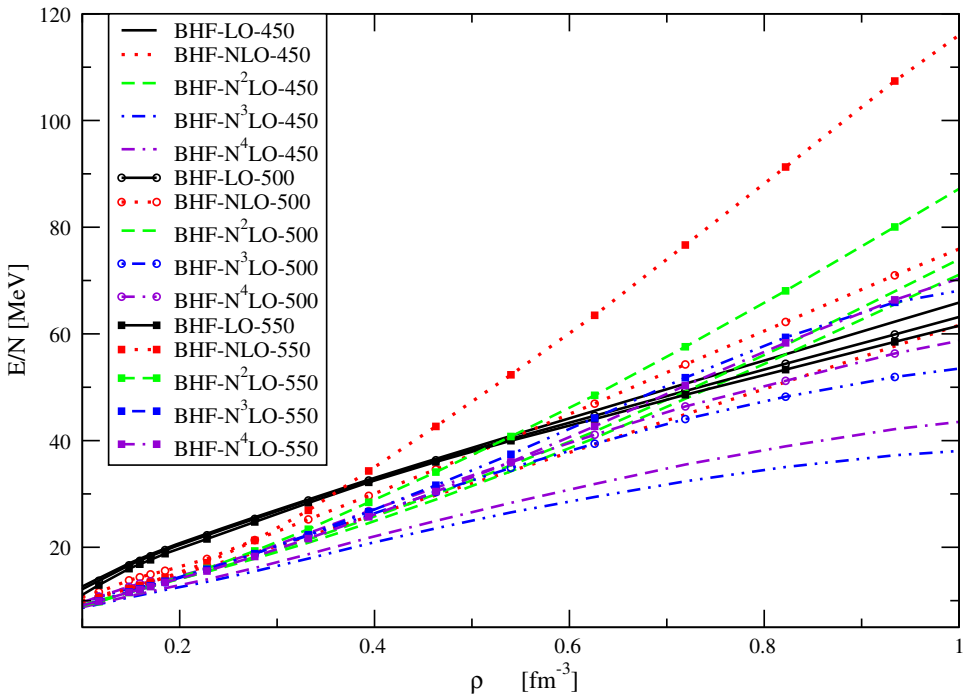

Figure 4. The EoS of PNM as a function of density using LO, NLO, N^2LO, N^3LO and N^4LO potentials at different momentum-space cut-off Λ. The predictions are obtained from BHF calculations.

Table 2. Contributions of various partial waves (in units of MeV) to the binding energies of PNM at $\rho = 0.16$ fm^{-3} for chiral NLO and N^{2}LO potentials applying for $\Lambda = 450$, 500 and 550 MeV.

Channel	BHF (450 MeV)	BHF (500 MeV)	BHF (550 MeV)
NLO			
$^1S_0$	−11.3	−11.3	−11.28
$^3P_0$	−2.25	−2.23	−2.19
$^3P_1$	5.75	5.63	5.38
$^1D_2$	−1.11	−1.12	−1.14
$^3F_2$	−0.28	−0.28	−0.288
$^3P_2$	−4.41	−3.62	−4.35
$^3F_3$	0.8	0.82	0.83
$^1G_4$	−0.212	−0.216	−0.22
$^3H_4$	0.15	−0.04	−0.04
$^3F_4$	−0.1	0.104	−0.1088
E/A	8.94	9.54	8.69
N^{2}LO			
$^1S_0$	−11.27	−11.25	−11.28
$^3P_0$	−2.12	−2.2	−2.19
$^3P_1$	5.85	5.69	5.59
$^1D_2$	−1.52	−1.54	−1.55
$^3F_2$	−0.32	−0.32	−0.32
$^3P_2$	−4.88	−4.77	−4.74
$^3F_3$	0.8	0.8	0.8
$^1G_4$	−0.23	−0.23	−0.23
$^3H_4$	0.042	−0.04	−0.042
$^3F_4$	−0.16	−0.166	−0.168
E/A	8.2	8.07	7.99

total binding energies mainly comes from the $^3S_1 - {}^3D_1$ channel [62].

In figure 5, we show pressure as a function of density ρ, for PNM and employing recent high-quality NN potentials from leading order to fifth order using BHF and BHF+CT which are then compared with the experimental data. The experimental data were provided by Danielewicz *et al* [63]. The area within the solid lines indicates that the EoS is consistent with the elliptic flow measurements which have been reported in that work. The two pressure contours in figure 5 correspond to the strongest (higher contour) and the weakest (lower contour) density dependence for nuclear symmetry energy proposed by Prakash and co-workers [64]. It turns out that the pressure calculated from BHF approach is in disagreement with the experimental values in the case of PNM. This is mainly due to the fact that BHF yields soft EoS. The present work clearly indicates that the use of BHF with CT is in very good agreement with the experimental and theoretical calculations for pressure. One can see that the contribution of the CT is fundamental especially at high density, and therefore an accurate inclusion of the TBF or CT is highly essential.

In figure 6, we show pressure as a function of density calculated in the BHF approximation using NLO potential at momentum-space cut-off values $\Lambda = 450$, 500 and 550 MeV respectively. The differences between various pressures are smaller in PNM especially at low and medium densities. These differences are significant at high densities.

The nucleon effective mass m^* describes the nonlocality of the single-particle potential felt by a nucleon propagating in the nuclear medium. Figure 7 shows the values of the effective mass as a function of density calculated in the three cases of the momentum-space cut-off parameter $\Lambda = 450$, 500 and 550 MeV using NLO potential. In the three cases, the effective masses are monotonically decreasing functions of density, whereas the inclusion of high momentum-space cut-off parameter Λ ($\Lambda = 550$ MeV) causes an increase in the values at high densities. The difference between the neutron effective mass at different values of Λ is shown to be small, especially at low and medium densities. Also it is seen indeed that the effective mass of PNM decreases much slower with density. Similar results have been reported by Baldo and co-workers [65].

Table 3. Same as table 2 but using N^3LO and N^4LO potentials.

Channel	BHF (450 MeV)	BHF (500 MeV)	BHF (550 MeV)
N^3LO			
$^1S_0$	− 11.45	− 11.32	− 11.27
$^3P_0$	− 2.09	− 2.03	− 2.07
$^3P_1$	5.71	5.79	5.82
$^1D_2$	− 1.57	− 1.53	− 1.56
$^3F_2$	− 0.34	− 0.34	− 0.34
$^3P_2$	− 4.84	− 4.43	− 4.51
$^3F_3$	0.79	0.79	0.78
$^1G_4$	− 0.236	− 0.237	− 0.237
$^3H_4$	0.04	− 0.04	− 0.04
$^3F_4$	− 0.21	− 0.21	− 0.22
E/A	7.8	8.44	8.06
N^4LO			
$^1S_0$	− 11.45	− 11.31	− 11.28
$^3P_0$	− 2.09	− 2.03	− 2.09
$^3P_1$	5.71	5.79	5.8
$^1D_2$	− 1.58	− 1.54	− 1.55
$^3F_2$	− 0.32	− 0.32	− 0.32
$^3P_2$	− 4.78	− 4.40	− 4.87
$^3F_3$	0.8	0.79	0.79
$^1G_4$	− 0.235	− 0.236	− 0.236
$^3H_4$	0.042	− 0.043	− 0.043
$^3F_4$	− 0.219	− 0.21	− 0.217
E/A	7.89	8.51	8.09

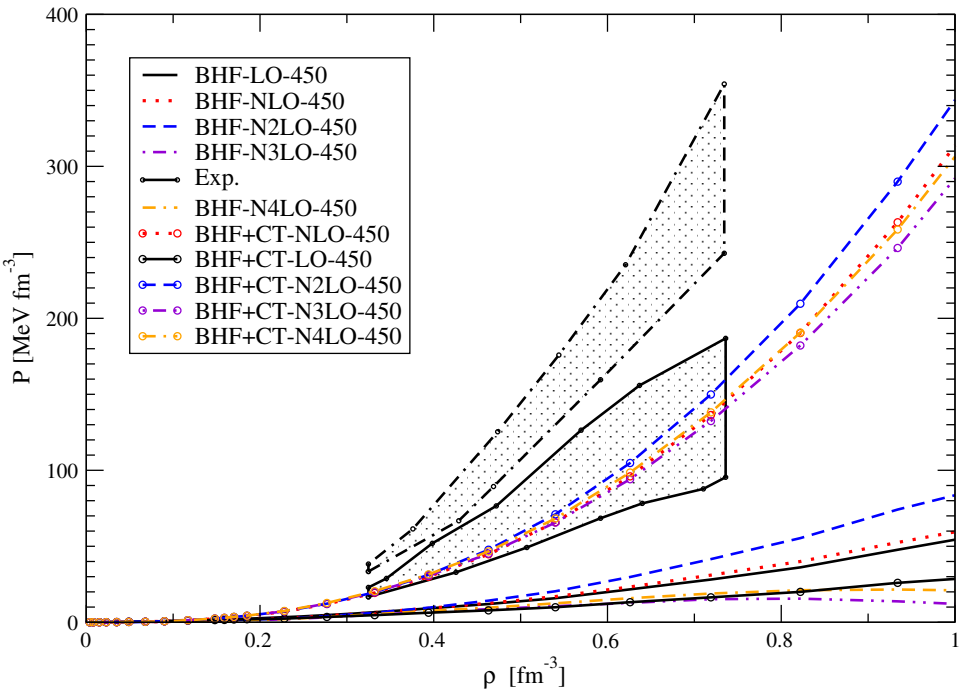

Figure 5. Pressure of PNM as a function of density using various potentials. The predictions are obtained from BHF and BHF+CT calculations. The two contours correspond to two parameterisations of the asymmetry term used in the analysis, as explained in the text [63].

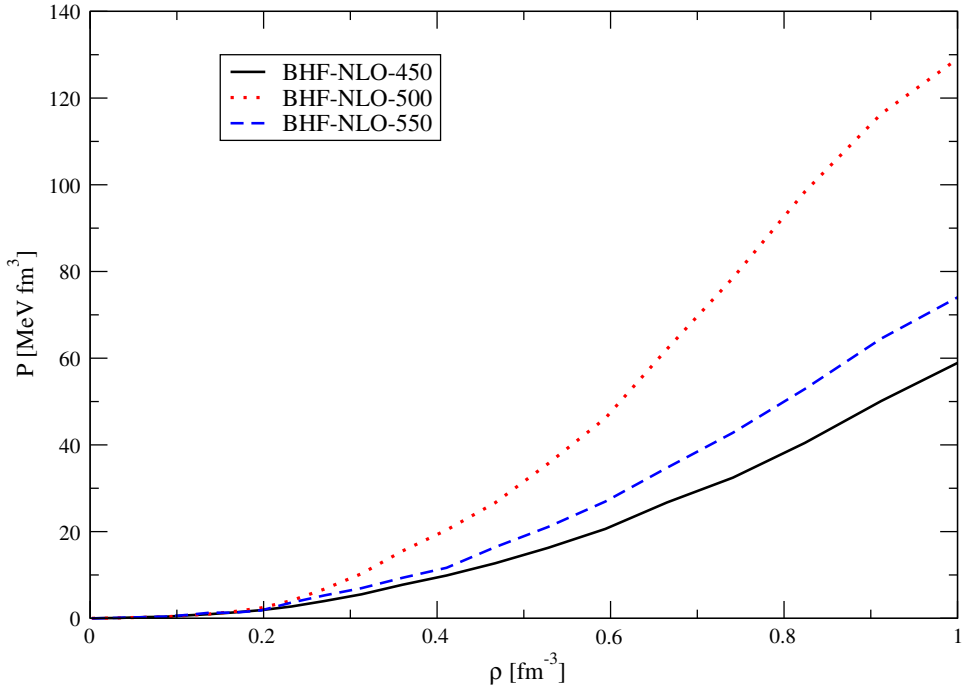

Figure 6. Pressure of PNM as a function of density using NLO potential at different momentum-space cut-off Λ. The predictions are obtained from BHF calculations.

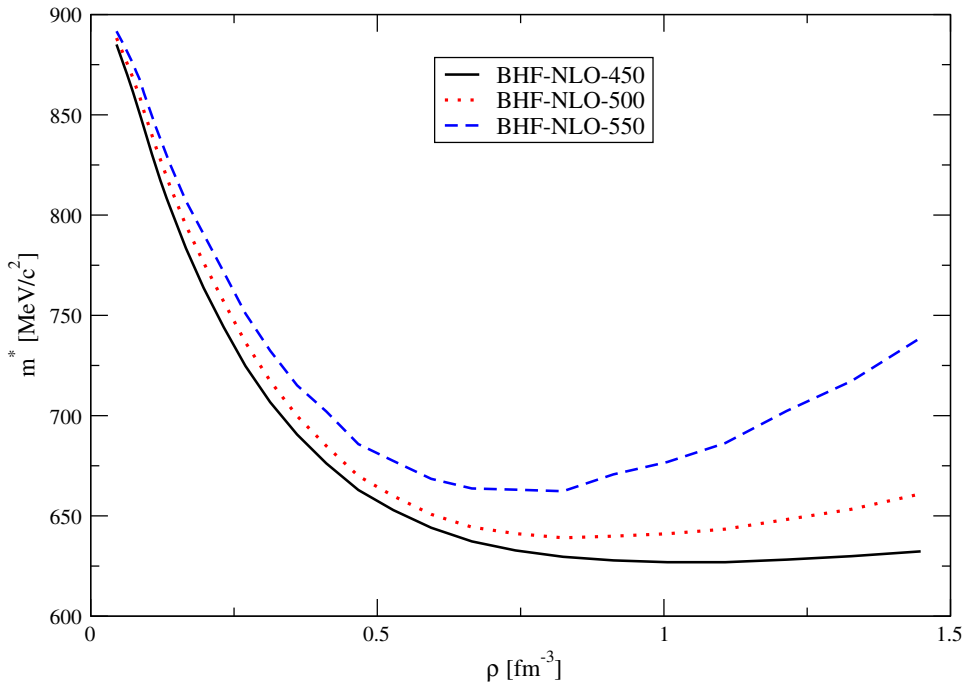

Figure 7. Effective mass m^* in PNM as a function of density ρ, using NLO potential at different momentum-space cut-off Λ. The predictions are obtained from BHF calculations.

The attractive nature of the neutron–neutron interaction at low momenta means the pressure must be soft at low density with rapid transition to a high pressure when the higher-momentum neutron–neutron interaction become important.

Baldo and co-workers [65] see that without TBF the values of the effective masses decrease with increasing nucleon density, whereas the inclusion of TBF causes an increase of the values at densities above 0.3 to 0.4 fm^{-3}. This is due to the repulsive character of the TBF

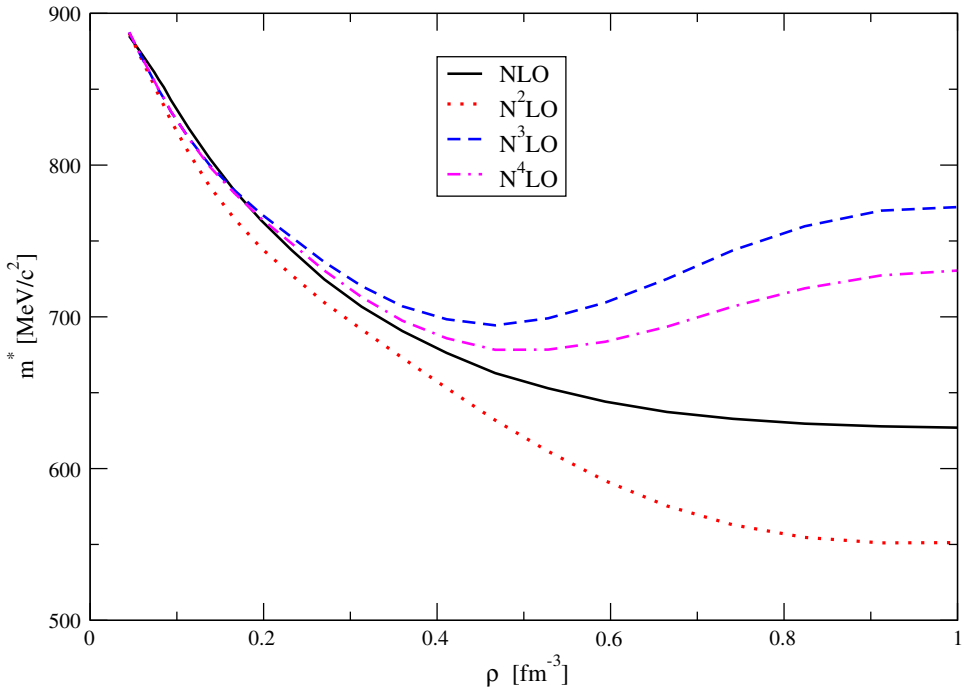

Figure 8. The calculated effective mass for neutron matter as a function of density at four orders of chiral perturbation theory. The predictions are obtained from BHF calculations. Λ is fixed at 450 MeV.

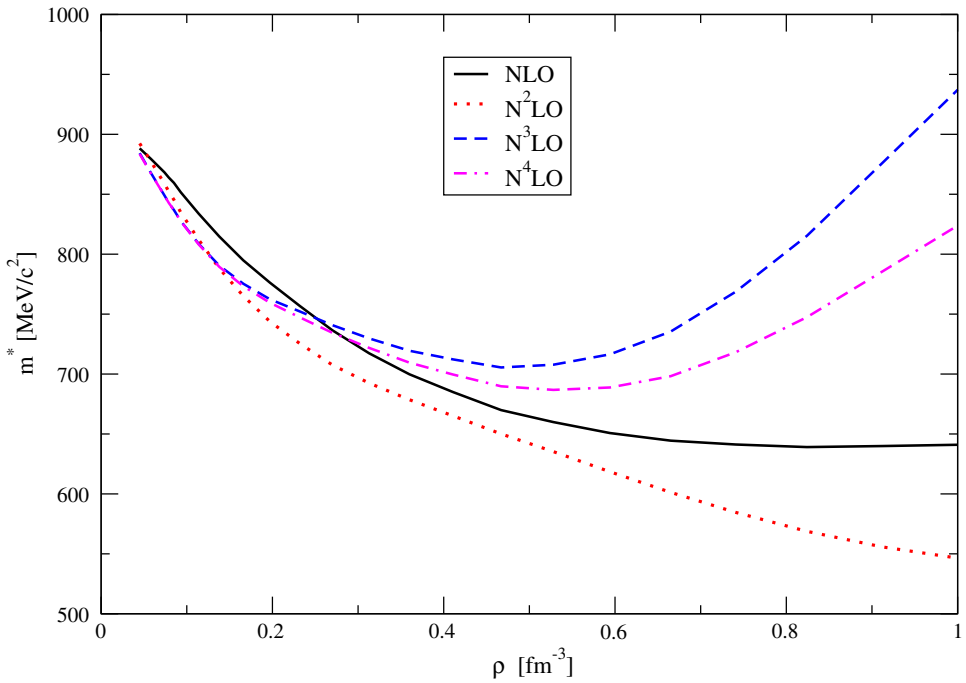

Figure 9. Same as figure 8 but using $\Lambda = 500$ MeV.

at high density. There is evidently a strong dependence on the chosen set of interactions, which reflects in particular the current theoretical uncertainty regarding nuclear TBF at high density. Using BHF+CT we got the same behaviour as seen in Baldo *et al* [65].

The calculated pressures are larger, if continuous values of single-particle potential without gap at Fermi momentum are employed, and the results are more sensitive to the details of the procedure to determine the effective mass m_n^* and constant C.

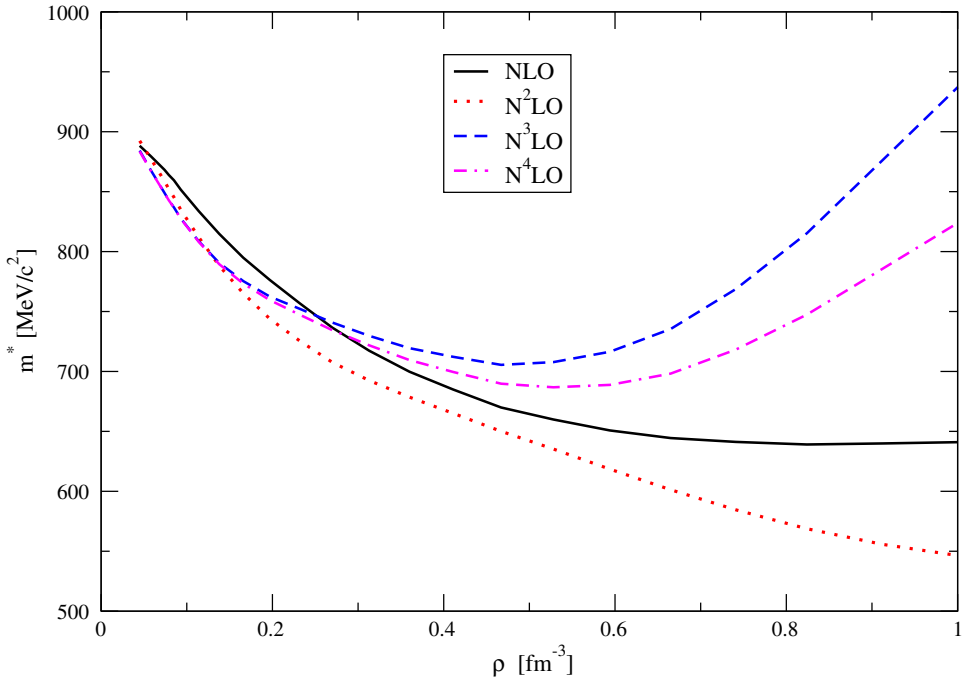

Figure 10. Same as figure 8 but using $\Lambda = 550$ MeV.

Figures 8–10 show the values of the effective mass as a function of density calculated for $\Lambda = 450$, 500 and 550 MeV respectively, using four orders of chiral perturbation theory. In the three cases, the effective masses are monotonically decreasing with increasing neutron density, whereas at density above 0.6 fm^{-3} the N^{3}LO and N^{4}LO potentials, the effective mass increasing with increasing density. There is evidently a strong dependence on the chosen set of interactions. The difference between the neutron effective mass at different values of momentum-space cut-off is shown to be large, especially at high densities. Also it is seen indeed that the effective mass of PNM decreases much slower with density. Similar results have been reported by Baldo and co-workers [65] using Argonne V18 + TBF at densities above 0.3–0.4 fm^{-3}.

Also we found that, in the low density region, the NLO effective mass was larger than the N^{3}LO, whereas this is opposite at high densities, as the central correlation on kinetic energy played a more important role at high densities than with the correlation on potential.

In table 4, the density behaviour of the energy per neutron of PNM is calculated in the BHF approach using LO, NLO, N^{2}LO, N^{3}LO and N^{4}LO potentials at $\Lambda = 450$ MeV.

4. Conclusions

In this paper, we have established the EoS of PNM at zero temperature on the bases of the BHF and BHF+CT approximations. The calculations are performed for LO, NLO, N^{2}LO, N^{3}LO and N^{4}LO potentials, up to density $\rho = 1.5$ fm^{-3} using three different values of momentum-space cut-off $\Lambda = 450$, 500 and 550 MeV. It is found that the EoS is very sensitive to any change in the momentum-space cut-off Λ, especially at higher densities.

We see that in comparison to the analogous study in SNM [31], the PNM results display a much weaker cut-off dependence. This may be due to the absence of central isospin-0 partial waves, in PNM, which appear to be more sensitive to differences among interaction. Although there are still many open questions, such as the sensitivity of EoS on the cut-off regularisations, the role and importance of many-body force parameters contributes to the behaviour of the neutron matter at high densities. Work along these lines is in progress.

We presented a comparison of the energy per nucleon for neutron matter in the BHF, BHF+CT and BHF+TBF approaches. We found similar binding energies at low densities, but a stiffer EoS for BHF+TBF and BHF+CT

Table 4. Binding energy per neutron (in units of MeV) for PNM from the chiral TBF with $\Lambda = 450$ MeV at different densities ρ (fm^{-3}).

ρ	LO	NLO	N^{2}LO	N^{3}LO	N^{4}LO
0.004	1.713	1.535	1.490	1.385	1.427
0.008	1.837	2.457	2.375	2.435	2.406
0.015	2.681	3.616	3.437	3.413	3.420
0.023	4.420	4.599	4.325	4.252	4.249
0.035	5.372	5.716	5.289	5.189	5.221
0.049	7.969	7.048	6.491	6.284	6.357
0.068	9.739	8.288	7.599	7.279	7.361
0.090	11.735	9.477	8.699	8.223	8.329
0.117	14.194	10.873	10.031	9.325	9.480
0.148	16.982	12.501	11.639	10.605	10.829
0.159	17.807	13.020	12.141	11.003	11.254
0.170	18.653	13.568	12.672	11.420	11.702
0.185	19.791	14.331	13.418	11.996	12.322
0.228	22.562	16.400	15.400	13.530	13.978
0.277	25.635	18.985	17.870	15.501	16.114
0.332	28.956	22.073	20.855	17.887	18.700
0.394	32.671	25.759	24.540	20.696	21.771
0.463	36.624	29.785	28.954	23.553	24.937
0.540	40.860	34.295	34.242	26.542	28.324
0.626	45.541	39.278	40.454	29.436	31.861
0.719	50.708	44.908	47.841	32.371	35.501
0.822	56.183	50.969	56.119	35.049	38.932
0.934	62.293	57.711	65.543	37.255	42.148
1.055	68.840	64.889	75.696	38.718	44.647
1.187	75.943	72.620	86.232	39.931	47.088
1.329	83.634	80.944	96.877	41.849	50.167
1.483	91.732	89.674	107.208	45.745	55.067

calculations at higher densities. The repulsion given by the addition of TBF is equivalent to the repulsion given by the addition of CT. This shows that our BHF+CT model is successful.

The contribution of CT is repulsive, leading to larger energies for BHF+CT compared to BHF. This repulsive effect is stronger in symmetric nuclear matter than in PNM [66,67]. This means that, the contribution of ladder diagrams is larger in the proton–neutron interaction than in the neutron–neutron interaction. Also the resulting EoS for pure neutron matter is in good agreement with the advanced many-body calculations over large density ranges.

Several extensions of the present model to include quark degrees of freedom and TBF are indeed under consideration. Also, the inclusion of thermal effects is on, which is necessary for applications and consistent neutron star merger simulations.

Finally, we have observed a reduced dependence on Λ, especially at low density. The differences in the prediction of the EoS at high densities are caused not only by the many-body method used or by momentum cut-off parameter, but also from the various models used for the NN interaction.

The good perturbative behaviour is independent of the choice of Λ, as well as the chiral order at which the nuclear potentials have been derived.

Acknowledgements

The author is grateful to Deanship of Scientific Research at Islamic University of Madinah for funding this work through the research Project No. (23/40) of the 10th (Takamul) programs of academic year 1440-1441 AH. The author would like to thank Professor R Machleidt for providing potential code.

References

[1] P Demorest, T Pennucci, S Ransom, M Roberts and J Hessels, *Nature* **467**, 1081 (2010)
[2] J Antoniadis *et al*, *Science* **340**, 6131 (2013)
[3] R Oechslin, H T Janka and A Marek, *Astron. Astrophys.* **467**, 395 (2007)
[4] R Oechslin and H T Janka, *Phys. Rev. Lett.* **99**, 121102 (2007)

[5] Y I Shin, C H Schunck, A Schirotzek and W Ketterle, *Nature* **689**, 451 (2008)
[6] M J H Ku, A T Sommer, L W Cheuk and M W Zwierlein, *Science* **563**, 335 (2012)
[7] Y LeCun, Y Begio and G E Hinton, *Nature* **521**, 436 (2015)
[8] D Kasen, B Metzger, J Barnes, E Quataert and E Ramirez-Ruiz, *Nature* **551**, 80 (2017)
[9] LIGO Scientific, Virgo: B P Abbott *et al*, *Phys. Rev. Lett.* **121**, 161101 (2018)
[10] E Annala, T Gorda, A Kurkela and A Vuorinen, *Phys. Rev. Lett.* **120**, 172703 (2018)
[11] I Bombaci and D Logoteta, *Astron. Astrophys.* **609**, A128 (2018)
[12] Y Fujimoto, K Fukushima and K Murase, *Phys. Rev. D* **101**, 054016 (2020)
[13] J M Lattimer and M Prakash, *Astrophys. J.* **550**, 426 (2001)
[14] J M Lattimer and M Prakash, *Science* **304**, 536 (2004)
[15] J M Lattimer and M Prakash, *Phys. Rep.* **442**, 109 (2007)
[16] F J Fattoyev, W G Newton, J Xu and B-A Li, *Phys. Rev. C* **86**, 025804 (2012)
[17] T Krüger, I Tews, B Friman, K Hebeler and A Schwenk, *Phys. Lett. B* **726**, 412 (2013)
[18] T Krüger, I Tews, K Hebeler and A Schwenk, *Phys. Rev. C* **88**, 025802 (2013)
[19] J M Dong, U Lombardo and W Zuo, *Phys. Rev. C* **87**, 062801(R) (2013)
[20] I Tews, T Krueger, K Hebeler and A Schwenk, *Phys. Rev. Lett.* **110**, 032504 (2013)
[21] I Tews, T Krüger, A Gezerlis, K Hebeler and A Schwenk, *Proceedings of the International Conference on Nuclear Theory in the Supercomputing Era 2013* (Iowa State University, May 13–17, 2013)
[22] H Heiselberg and M Hjorth-Jensen, *Phys. Rep.* **328**, 237 (2000)
[23] N K Glendenning, *Phys. Rep.* **342**, 393 (2001)
[24] M Baldo, I Bombaci and G F Burgio, *Astron. Astrophys.* **328**, 274 (1997)
[25] R Schiavilla, V R Pandharipande and R B Wiringa, *Nucl. Phys. A* **449**, 219 (1986)
[26] J Carlson, R R Pandharipande and R B Wiringa, *Nucl. Phys. A* **401**, 59 (1983)
[27] R Machleidt and D R Entem, *Phys. Rep.* **503**, 1 (2011)
[28] E Marji, A Canul, Q Macpherson, R Winzer, Ch Zeoli, D R Entem and R Machleidt, *Phys. Rev. C* **88**, 054002 (2013)
[29] F Sammarruca, R Machleidt and N Kaiser, *Phys. Rev. C* **92**, 054327 (2015)
[30] D R Entem, R Machleidt and Y Nosyk, *Phys. Rev. C* **96**, 024004 (2017)
[31] F Sammarruca, L E Marcucci, L Coraggio, J W Holt, N Itaco and R Macheidt, arXiv:1807.06640v1
[32] M Hoferichter, J Ruiz, de Elvira, B Kubis and U-G Meissner, *Phys. Rev. Lett.* **115**, 192301 (2015); *Phys. Rep.* **625**, 1 (2016)
[33] J P Jeukenne, A Lejeune and C Mahaux, *Phys. Rev. C* **10**, 1391 (1974)
[34] H Q Song, M Baldo, G Giansiracusa and U Lombardo, *Phys. Rev. Lett.* **81**, 1584 (1998)
[35] Kh Gad, *Eur. Phys. J. A* **22**, 405 (2004)
[36] K Gad, *Nucl. Phys. A* **747**, 655 (2005)
[37] K Gad, *J. Phys. G* **32**, 799 (2006)
[38] K Gad and K S A Hassaneen, *Nucl. Phys. A* **793**, 67 (2007)
[39] K Hassaneen and K Gad, *J. Phys. Soc. Jpn.* **77**, 084201 (2008)
[40] P Gögelein, E N E Van Dalen, K Gad, K S A Hassaneen and H Müther, *Phys. Rev. C* **79**, 024308 (2009)
[41] H Mansour, K Gad and K S A Hassaneen, *Prog. Theor. Phys.* **123**, 687 (2010)
[42] K Gad, *Ann. Phys.* **326**, 2474 (2011)
[43] K Gad, *Ann. Phys.* **327**, 2403 (2012)
[44] F Coester, S Cohen, B D Day and C M Vincent, *Phys. Rev. C* **1**, 769 (1970)
[45] S Gandolfi, A Gezerlis and J Carlson, *Annu. Rev. Nucl. Part. Sci.* **65**, 303 (2015)
[46] T H R Skyrme, *Nucl. Phys.* **9**, 615 (1959]
[47] D Vautherin and D M Brink, *Phys. Rev. C* **5**, 62 (1972)
[48] P Bonche and D Vautherin, *Nucl. Phys. A* **372**, 496 (1981)
[49] J R Stone and P-G Reinhard, *Prog. Part. Nucl. Phys.* **56**, 587 (2007)
[50] I Dutt and N K Dhiman, *Chin. Phys. Lett.* **27**, 112401 (2010)
[51] E Chabanat, P Bonche, P Haensel, J Meyer and R Schaeffer, *Nucl. Phys. A* **627**, 710 (1997); *Nucl. Phys. A* **635**, 231 (1998)
[52] E N E van Dalen, P Gögelein and H Müther, *Phys. Rev. C* **80**, 044312 (2009)
[53] P Grygorov, E N V van Dalen, J Margueron and H Müther, *Phys. Rev. C* **82**, 014315 (2010)
[54] E N E van Dalen and H Müther, *Phys. Rev. C* **90**, 034312 (2014)
[55] P Grange, J Cugnon and A Lejeune, *Nucl. Phys. A* **473**, 365 (1987)
[56] G Q Li, R Machleidt and R Brockmann, *Phys. Rev. C* **45**, 2782 (1992)
[57] S Gandolfi, J Carlson, S Reddy, A W Steiner and R B Wiringa, *Eur. Phys. J. A* **50**, 10 (2014)
[58] A Akmal, V R Pandharipande and D G Ravenhall, *Phys. Rev. C* **58**, 1804 (1998)
[59] R Millerson and F Sammarruca, arXiv:1906.02905v1
[60] S Binder, J Langhammer, A Calci and R Roth, *Phys. Lett. B* **736**, 119 (2014)
[61] K Gad, *Eur. Phys. J. A* **51**, 98 (2015)
[62] P Wang and W Zuo, *Chin. Phys. C* **33**, 1 (2009)
[63] P Danielewicz, R Lacey and W G Lynch, *Science* **298**, 1592 (2002)
[64] M Prakash, T L Ainsworth and J M Lattimer, *Phys. Rev. Lett.* **61**, 2518 (1988)
[65] M Baldo, G F Burgio, H-J Schulze and G Taranto, *Phys. Rev. C* **89**, 048801 (2014)
[66] K Gad, *Phys. At. Nucl.* **81**, 429 (2018)
[67] K Gad, *Indian J. Phys.* **95**, 1499 (2021)